Atomic structure and conduction mechanism of hydrous RuO_2

4 AUTHORS, INCLUDING:

Takeshi Egami
University of Tennessee
545 PUBLICATIONS **12,152** CITATIONS

SEE PROFILE

Karen E. Swider-Lyons
United States Naval Research Laboratory
105 PUBLICATIONS **1,531** CITATIONS

SEE PROFILE

Local Atomic Structure and Conduction Mechanism of Nanocrystalline Hydrous RuO₂ from X-ray Scattering

Wojtek Dmowski* and Takeshi Egami

Department of Materials Science and Engineering and the Laboratory for Research on the Structure of Matter, University of Pennsylvania, Philadelphia, Pennsylvania 19104

**Karen E. Swider-Lyons, Corey T. Love, and Debra R. Rolison**

Code 6170, Naval Research Laboratory, Washington, DC 20375-5342

*Received: June 3, 2002; In Final Form: September 18, 2002*

Hydrous ruthenium oxide ($RuO_2 \cdot xH_2O$ or RuO_xH_y) is a mixed proton−electron conductor which could be used in fuel cells and ultracapacitors. Its charge-storage (pseudocapacitance) and electrocatalytic properties vary with water content and are maximized near the composition $RuO_2 \cdot 0.5$ mol % H_2O. We studied the atomic structure of $RuO_2 \cdot xH_2O$ as a function of water content from $x = 0.84$ to 0.02 using X-ray diffraction and atomic pair density function (PDF). Even though the diffraction patterns of samples containing 0.84 to 0.35 mole of water are suggestive of "amorphous" structures, the PDF analysis clearly shows that up to 0.7 nm, the short-range atomic structure of all of these $RuO_2 \cdot xH_2O$ samples resembles that of the anhydrous rutile RuO_2 structure. We conclude that $RuO_2 \cdot xH_2O$ is a composite of anhydrous rutile-like RuO_2 nanocrystals dispersed by boundaries of structural water associated with Ru−O. Metallic conduction is supported by the rutile-like nanocrystals, while proton conduction is facilitated by the structural water along the grain boundaries. This structural picture explains the charge-storage and electrocatalytic properties of $RuO_2 \cdot xH_2O$ in terms of competing percolation networks of metallic and protonic conduction pathways, that vary in volume as a function of the water content of the $RuO_2 \cdot xH_2O$. The control and optimization of electron and proton conducting volumes and pathways will lead to improved performance and guide the design of new materials.

Introduction

Hydrous ruthenium dioxide, $RuO_2 \cdot xH_2O$ or RuO_xH_y, is a mixed electronic−protonic conductor.[1,2] $RuO_2 \cdot xH_2O$ is used as a charge-storage medium in ultracapacitors,[3,4] and as an electrocatalyst in dimensionally stable anodes for chlorine evolution[5,6] and in combination with Pt in direct-methanol fuel cells (DMFC) anodes.[7,8] The electrochemical and electrocatalytic properties of this material depend on the amount of water in its structure. Optimum pseudocapacitance and electrocatalytic activity is achieved when $RuO_2 \cdot xH_2O$ is heated at ∼150 °C to yield $x \sim 0.5$ mole of H_2O.[3,9] The charge storage mechanism is explained by the "double insertion" of electrons and protons into the structure, as expressed in eq 1:[5,6]

$$RuO_x(OH)_y + \delta H^+ + \delta e^- \Leftrightarrow RuO_{x-\delta}(OH)_{y+\delta} \qquad (1)$$
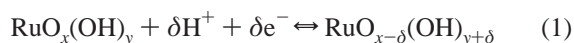
As a result of charge infusion, the oxidation state of ruthenium is expected to change between Ru^{4+}, Ru^{3+}, and Ru^{2+}, as expressed in eq 2

$$Ru^{4+} - O + H^+ + e^- \Leftrightarrow Ru^{3+} - OH \qquad (2)$$
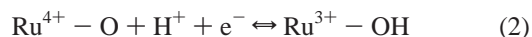
for the Ru^{4+}/Ru^{3+} couple.[10]

Equations 1 and 2 imply that the $RuO_2 \cdot xH_2O$ is an ionic compound, with protons inserting in the lattice. However, $RuO_2 \cdot xH_2O$ is a metallic conductor,[11] and cyclic voltammetry shows nearly constant current vs voltage and weak evidence of distinct charge couples, implying that the electrons are fully or partially delocalized and there are no discrete ions.[11]

These unusual electrochemical properties of $RuO_2 \cdot xH_2O$ should be related to the atomic structure of the material. The knowledge of the atomic structure would help not only to reconcile different experimental evidences but also to optimize desired electrochemical properties. Unfortunately the apparent "amorphousness" of the hydrous oxide has made it difficult to establish such a correlation. Standard crystallographic methods that rely upon the analysis of the Bragg peaks are not useful for this material because diffraction peaks are broad and diffuse. While the X-ray absorption fine structure (EXAFS or XAFS) method can be used as a local structural probe and provide information about the immediate local environment of Ru,[2] EXAFS cannot shed light on the intermediate-range structure from 0.3 to 1.5 nm.

Atomic pair-density function (PDF) analysis is an alternative approach for examining the local and medium-range structures of materials. PDF has been widely used in the studies of glasses and liquids[13] and has also been applied successfully to characterize local and defect structures of crystalline solids as well as other complex inhomogeneous systems.[14] Using this method, we demonstrate in this paper that the medium-range structure of $RuO_2 \cdot xH_2O$ is highly inhomogeneous, and it is best described as a network of ruthenium oxide nanocrystals dispersed by boundaries of structural water associated with Ru−O. The size of the ruthenium oxide nanocrystals changes with the water content in the structure. On the basis of this result we propose a model of parallel percolative conduction mechanisms in which

---

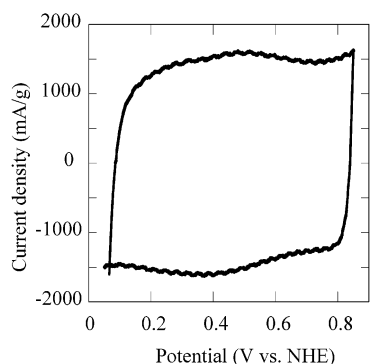* Corresponding author. E-mail: dmowski@lrsm.upenn.edu.

12678 *J. Phys. Chem. B, Vol. 106, No. 49, 2002*

Dmowski et al.

Figure 1. A cyclic voltammagram of $RuO_2 \cdot 0.58H_2O$ measured in 0.5 M H_2SO_4 at a sweep rate of 2 mV/s.

TABLE 1: Pseudocapacitance of $RuO_2 \cdot xH_2O$ vs Structural Water Content, x

annealing temperature (°C)	$RuO_2 \cdot xH_2O$ x mole %H_2O ± 7%	pseudocapacitance (F/g) ± 4.8%
25	2.11	505
100	0.84	740
150	0.58	850
169	0.48	735
200	0.35	365
300	0.14	250
400	0.02	125

the connectivity of ruthenium oxide and hydrous matrix controls the electron and proton conduction in the system, respectively.

Experimental Details and Results

Samples. Commercial hydrous ruthenium dioxide powder, $RuO_2 \cdot xH_2O$ (Alfa Aesar) is used as received or after heating in porcelain crucibles for 18 h at selected temperatures between 100 and 400 °C. The water content of the materials is estimated from the amount of weight lost from the materials at 450 °C under flowing Ar (Rheometric Scientific Simultaneous Thermal Analyzer). Commercial anhydrous RuO_2 (Alfa Aesar) was used as a standard.

Electrochemical Characterization. For electrochemical evaluation, the $RuO_2 \cdot xH_2O$ was mixed with 5 wt % Teflon powder and pressed at 1100 psi onto porous carbon paper (Toray).[3] The $RuO_2 \cdot xH_2O$ on carbon paper was cycled at 2 mV/s in deaerated 0.5 M H_2SO_4 vs a Pt mesh auxiliary electrode and a Pd/H normal hydrogen reference electrode (NHE) using a programmable potentiostat (EG&G PAR 263). The pseudocapacitance was calculated from the average current of the charging sweep between 0.2 and 0.8 V vs NHE. The pseudocapacitance of the $RuO_2 \cdot xH_2O$ samples vs water content is summarized in Table 1. The water content varies from $x = 2.11$ to 0.02. These results are consistent with results reported elsewhere,[2,3] and the $RuO_2 \cdot xH_2O$ exhibits a maximum in its pseudocapacitance of 850 F/g when annealed at 150 °C and has the composition $RuO_2 \cdot 0.58 H_2O$. A cyclic voltammagram of $RuO_2 \cdot 0.58H_2O$ is shown in Figure 1. The current is virtually independent of voltage between 0.2 and 0.8 V vs NHE and there are no obvious electrochemical couples, suggesting that the electrons are being inserted uniformly into a metal band. The cyclic voltammagrams for all $RuO_2 \cdot xH_2O$ samples with $x = 2.11$ and 0.02 are similar, and only vary in their area.

Powder X-ray Diffraction. The powder XRD patterns of the $RuO_2 \cdot xH_2O$ were measured for 2θ between 10 and 60° with Cu Kα radiation ($\lambda = 0.15418$ nm) at 40 kV and 40 mA (Bruker D8 Advance Diffractometer with Göbel mirrors). Figure 2 presents the XRD patterns for three $RuO_2 \cdot xH_2O$ samples with
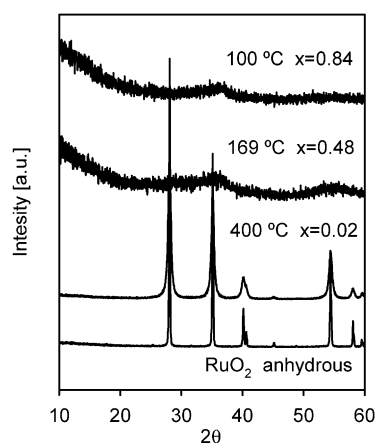

Figure 2. X-ray diffraction patterns of $RuO_2 \cdot xH_2O$ (with $x = 0.0, 0.02, 0.48, 0.84$) measured with Cu K$\alpha$ radiation ($\lambda = 0.15418$ nm).

different water contents ($x = 0.02, 0.48, 0.84$ annealed at 400, 169, and 100 °C, respectively) measured with Cu Kα radiation. The standard XRD experiment with Cu Kα radiation shows only diffuse scattering for samples annealed at less than 200 °C. The peaks are sharp for the sample annealed at 400 °C and match well to anhydrous RuO_2, indicating long-range crystalline order. This figure illustrates a common problem with a structural characterization of complex materials: diffraction patterns appear to be either crystalline or amorphous, suggesting extreme changes in the atomic ordering. Samples heated at 169 °C and 100 °C can be thought of as "amorphous", and therefore strongly disordered, while samples heated at 400 °C are considered crystalline. On the basis of such differences in the diffraction patterns, it could be surmised that a high concentration of water in the metal oxides leads to a collapse of the crystalline order and formation of an "amorphous" structure. However, as we demonstrate here such an assumption is erroneous.

Synchrotron X-ray Scattering. Synchrotron X-ray scattering measurements are performed at the beamline X7A of the National Synchrotron Light Source. Diffraction patterns from the powder samples are measured in the symmetric reflection geometry with the incident X-ray wavelength (λ) of 0.0574 nm. Flat plate samples are enclosed in He-filled chamber with Kapton film windows. The data are measured up to 200 nm^{-1} in the scattering vector Q ($Q = 4\pi \sin \theta/\lambda$, where θ is the scattering angle) using a solid-state Ge detector. On average, 6×10^5 total counts are collected per 10 nm^{-1}. Measured intensities are corrected for the background scattering, absorption, polarization, multiple scattering, and inelastic (Compton) scattering to obtain the normalized total scattering function, $S(Q)$. The pair-density function (PDF), $\rho_0 g(r)$, (where $g(r)$ is a pair distribution function and ρ_0 denotes atomic density), is obtained by the direct Fourier transformation of the total scattering function including both the Bragg peaks and diffuse scattering intensities (eq 3).

$$\rho_0 g(r) = \rho_0 + \frac{1}{2\pi^2 r} \int_0^\infty [S(Q) - 1]\sin (Qr)Q \, dQ \quad (3)$$

The atomic pair-density function gives direct information, albeit one-dimensional, about the distribution of the interatomic distances. The theoretical and experimental procedures are described elsewhere.[12−14]

Figure 3 presents X-ray scattering functions $S(Q)$ (structure factors) for three samples.[11] The two samples with high water contents ($x = 0.48$ and 0.84) exhibit strong diffuse scattering patterns, with additional superimposed sharp peaks, indicating
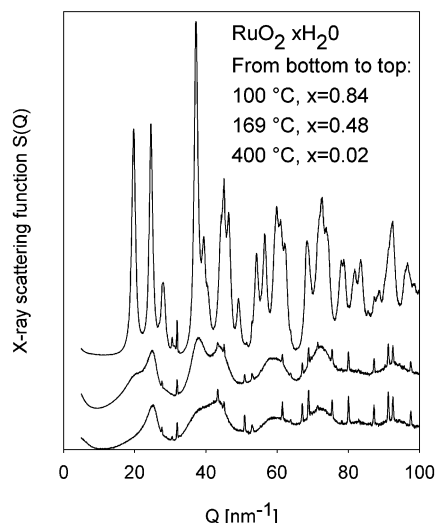
Nanocrystalline Hydrous RuO$_2$

J. Phys. Chem. B, Vol. 106, No. 49, 2002 **12679**

Figure 3. Normalized X-ray scattering functions $S(Q)$ of RuO$_2$·xH$_2$O (with $x = 0.02, 0.48, 0.84$) as a function of the scattering vector Q ($Q = 4\pi \sin \theta/\lambda$, where θ is the scattering angle and $\lambda = 0.0574$ nm).
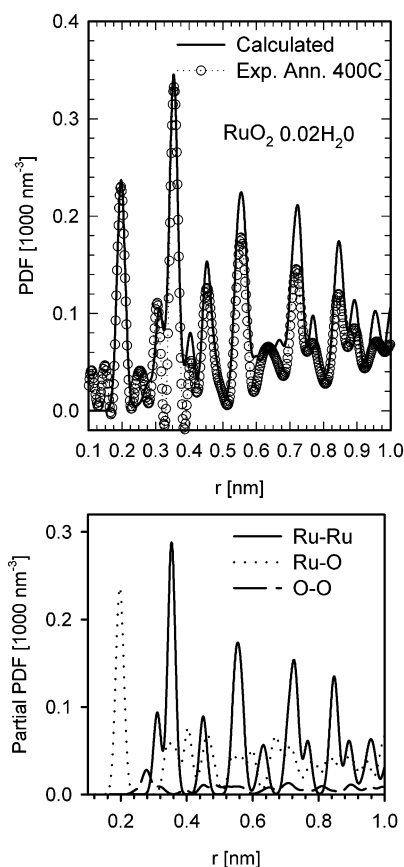

Figure 4. (a) The atomic pair distribution function (PDF) for RuO$_2$·0.02H$_2$O, heated at 400 °C, compared with a theoretical PDF for RuO$_2$ calculated from an ideal rutile structure. (b) The partial atomic PDFs for RuO$_2$ calculated from an ideal rutile structure.

the presence of a small volume of anhydrous RuO$_2$. The scattering pattern for RuO$_2$·0.02H$_2$O has sharp Bragg peaks, and, like the data in Figure 2, indicating that the material is crystalline. Figure 4a displays the PDF for RuO$_2$·0.02H$_2$O obtained from the scattering pattern in Figure 3 and the Fourier transform in eq 3. For comparison, a model PDF is calculated from the rutile RuO$_2$ structure[15] (shown in Figure 5). The partial distribution functions that illustrate contributions of Ru−Ru, Ru−O, and O−O pairs to the model PDF are given in Figure
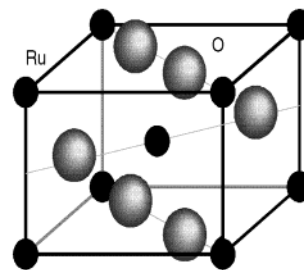

Figure 5. The rutile structure of RuO$_2$ (space group $P4_2/mnm$, $a = 0.4919$ nm, $c = 0.31066$ nm).

4b. In the tetragonal unit cell of RuO$_2$, Ru atoms occupy the corners and the body center. The oxygen atoms are on the $z = 0$ plane at $(u, -u, 0)$ and $(-u, u, 0)$ positions and on the $z = 1/2$ plane at $(1/2 - u, 1/2 - u, 1/2)$ and $(-1/2 + u, 1/2 + u, 1/2)$ positions, with $u = \sim0.31$. A Ru atom is coordinated with 6 oxygen atoms, forming a distorted octahedron. There are four short and two long Ru−O distances at 0.194 and 0.198 nm, respectively. The oxygen octahedra share edges along the c-axis but only vertexes in the basal plane. The O octahedron around the Ru ion at the corner is rotated by 90 degrees with respect to the one at the center. The nearest distance between two Ru atoms is along the c-axis at 0.31 nm. The distance from the corner Ru to the body-centered Ru is 0.354 nm.

In Figure 4a, the peak positions and amplitudes agree well between the experimental PDF determined for the RuO$_2$·0.02H$_2$O sample and the PDF calculated for anhydrous RuO$_2$, indicating that the rutile structure is largely maintained in the sample. The oscillations in the measured PDF become damped in amplitude with increasing interatomic distance (r) faster than the model PDF, suggesting that the crystalline size may be rather small even after annealing at 400 °C. Indeed the widths of diffraction peaks suggest an average crystallite size of 6−7 nm. In Figure 4a, the ripple peaks on both sides of the 0.20 nm peak are the effects of the Fourier transformation termination and normalization errors.

We can readily identify major peaks in the PDF of the RuO$_2$·0.02H$_2$O sample in Figure 4a on the basis of comparison to the rutile structure (Figure 5). Because Ru has a larger number of electrons, Z, than oxygen and the X-ray scattering cross-section depends on Z^2, the PDF is weighted significantly by the Ru−Ru and Ru−O correlations, as illustrated by the X-ray weighted partial PDF shown in Figure 4b. The peak at 0.196 nm corresponds to the Ru−O distance in the RuO$_6$ octahedron in the rutile structure. The integrated area of this peak corresponds to an average number of 5.6 ± 0.5 O atoms around each Ru atom, which suggests that most of the Ru ions are fully 6-coordinated. Surface termination or other structural defects may reduce the average coordination number. The peak near 0.31 nm is due to the nearest distance along the c-axis (c-axis parameter in the rutile structure), which is dominated by Ru−Ru pairs plus some overlap from the O−O (~ 0.28 nm) separation along the edges of the octahedron. The second-shell Ru−Ru distance at 0.354 nm is between the body center and the corner Ru atoms. The peak at 0.449 nm corresponds to the tetragonal a-axis length and at 0.555 nm to a−c face diagonal. Both peaks are heavily weighted by Ru−Ru because of the large Z of the Ru compared to the O atom as shown by the partial PDFs in Figure 4b.

The good agreement between the experimental and model PDFs in Figure 4a, in particular for the Ru sub-lattice peaks, suggests that the core structure of RuO$_2$·0.02H$_2$O is close to that of the ideal rutile structure. However, there are some

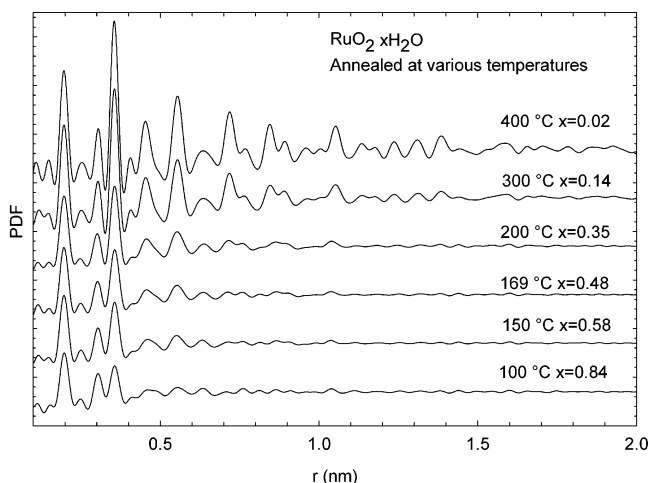**Figure 6.** PDFs for $RuO_2 \cdot xH_2O$ with various structural water contents ($x = 0.02$ to 0.84).

Figure 7. Full width at half-maximum (fwhm) of several PDF peaks for $RuO_2 \cdot xH_2O$ as function of the amount of structural water, x.

indications of deviations in the oxygen sub-lattice. For example, the width of the Ru−O peak at 0.196 nm is wider than expected from the model rutile unit cell. Most discrepancies in the peak positions in Figure 4a are observed to the left and right of 0.354 and 0.64 nm peaks, near the Ru−O distances in the ideal rutile structure. These discrepancies suggest local structural deviations resulting from the shift of oxygen atoms from the ideal positions in the rutile structure or from some other structural defects in the sample. These deviations may not necessary indicate disorder. The crystallographic structure is frequently a compromise between strains forced by the long-range crystallographic order and local packing. If the long-range constraint is removed at the surface of small nanocrystals, the local structure can relax. For instance, the very short O−O distance of 0.247 nm, compared to the ideal ionic distance[16] of 0.28 nm, could indicate that these pairs of oxygen ions may be under compression, and become elongated at the surface.

The PDFs for samples with various water contents (from $x = 0.02$ to 0.84) are compared in Figure 6. For samples with $x > 0.35$, the PDF peaks at distances larger than 0.6 nm are reduced in height compared to $RuO_2 \cdot 0.02H_2O$, indicating gradual loss of long-range crystalline correlations. However, several peaks up to 0.5 nm are always present and the samples retain the local structure similar to the rutile crystal. This indicates that the samples, even with the highest water content ($x = 0.84$), are not amorphous, because in amorphous material all peaks beyond first shells should become broad.

The change in full width at the half-maximum (fwhm) of the selected PDF peaks are shown as a function of the structural water content in $RuO_2 \cdot xH_2O$ in Figure 7. The PDF peak widths are a function of the distribution of the interatomic distances. There is an intrinsic part due to thermal motions of the atoms around their average position in the structure plus a structural part that depends on the distribution of the contributing interatomic distances. As the interatomic distances become more distributed (or the structure becomes more disordered), the peak width increases and at the same time the peak height decreases. The peak height can also decrease, without change in width, by the loss of the contributing atoms (i.e., by termination at a surface or due to dispersion in grain size).

Discussion

Local Structure around Ru. We first examine the effect of water on the structure of $RuO_2 \cdot xH_2O$ by studying the changes in the position and width of the PDF peaks vs water content.
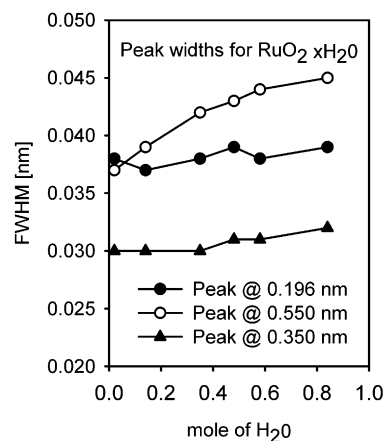
The position (Figure 6) and widths (Figure 7) of the PDF peaks yield the most information because they are least affected by experimental errors.

The PDF peak at 0.196 nm is due to the Ru−O distance within the RuO_6 octahedron. The position of this peak ($r = 0.196$ nm) remains unchanged for all the examined samples. Similarly the fwhm of this peak (0.038 nm) changes negligibly with water content. Thus we conclude that, as in the $RuO_2 \cdot 0.02H_2O$, most of the Ru ions are coordinated in RuO_6 octahedra, independently of the amount of structural water. The width of the 0.196 nm PDF peak, which is $\sim 30\%$ larger than expected from the intrinsic thermal motion, may result from the oxygen displacement from the ideal position in the rutile unit ($u = 0.303$), leading to a wider distribution of the Ru−O distances. There may be some difference in the arrangement of atoms in the oxygen octahedra due to crystallite size and extended surface.

The position the PDF peak at $r \sim 0.31$ nm (Figure 6) exhibits almost no dependence on the water content. This peak is dominated by the first shell Ru−Ru distances with small overlap coming from the O−O distances at ~ 0.28 nm (see Figure 4b). Thus, Ru atoms maintain both their nearest Ru neighbor and octahedral coordination. The positions of PDF peaks corresponding to the second and third shell Ru−Ru distances (at ~ 0.35 and ~ 0.55 nm) do not change with x, but widths of these peaks depend on the amount of structural water in the $RuO_2 \cdot xH_2O$ (Figure 7a). The width of the peak at $r = 0.35$ nm changes only slightly with x, but the width of the peak at $r = 0.55$ nm shows more pronounced changes, increasing from 0.037 for $x = 0.02$ to 0.045 nm fwhm for $x = 0.84$.

The results for the PDF peak position and fwhm indicate that the core atomic structure up to 0.5 nm remains essentially unchanged in the $RuO_2 \cdot xH_2O$ for $0.02 > x > 0.84$. For samples containing higher amounts of water, $x > 0.15$, the PDF peaks beyond 0.6 nm are more damped and broadened, indicating weaker atomic correlations.

Structure of $RuO_2 \cdot xH_2O$. From the observed variations in the PDF with x, it is possible to deduce a model for the structure of $RuO_2 \cdot xH_2O$. In general there are three possible scenarios describing structure of $RuO_2 \cdot xH_2O$ that should be considered. First the structure could be an isotropic "amorphous" solid. However, we have to exclude such a proposition since it is not consistent with PDF data which show that there is a definite local atomic arrangement very similar to the rutile structure in all of the $RuO_2 \cdot xH_2O$ samples. The positions and the widths of the first several PDF peaks are essentially independent of x, indicating that the local structure of the Ru atoms (up to 0.5
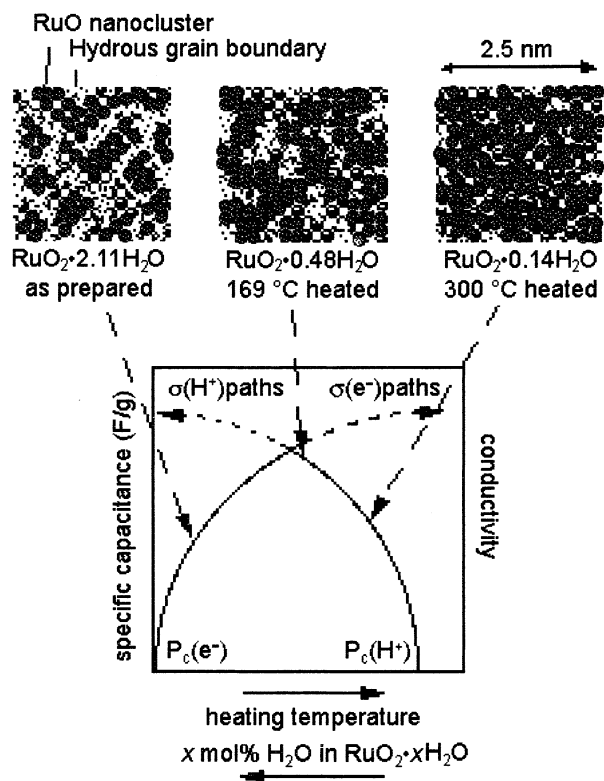
Figure 8. Schematic illustration of the variation of the percolation volumes of the RuO$_2$ nanocrystals and the hydrous grain boundaries with changes in water content.

nm) is the same as that of rutile RuO$_2$, and does not change much with x. In contrast, truly amorphous solids show much broader PDF peaks. For example, in amorphous silica, both Si–O bond and O–Si–O angle are well defined in the local tetrahedral unit, so that the first Si–O and O–O PDF peaks are sharp. However, the Si–O–Si bond angle is flexible, leading to broad first and second Si–Si peaks and formation of a continuous random network.[24] In the case of RuO$_2$·xH$_2$O, the first, second, and third Ru–Ru distances are well defined (see Figures 6 and 7). Distribution in the Ru–Ru distances is seen only beyond the 4th shell (beyond 0.55 nm).

The second structural possibility is that RuO$_2$·xH$_2$O is composed of a mixture of crystalline, anhydrous RuO$_2$ plus an "amorphous" hydrous RuO$_2$. Because PDF spans all Ru–Ru distances in the sample, we would expect to see the PDF peak consisting of narrow part that describes the distribution in the rutile-like particle and the broad part that corresponds to the "amorphous" part. Again we do not see such peaks in the PDF, precluding this second structural model.

Therefore, the third and most viable structural picture for RuO$_2$·xH$_2$O is a "nanocrystalline" model, which consists of nanometer-size crystals with extended low-density boundary regions. In this model, RuO$_2$·xH$_2$O is composed of assemblies of small rutile-like ruthenium oxide nanocrystals or clusters having water (or protons) that is chemisorbed and physisorbed on the surface of the grains (Figure 8). The broadening and damping of the PDF peaks (Figure 6) suggest that the ruthenium oxide nanocrystals are smaller and more dispersed for samples with high water contents, and can be as small as ∼1.2–2.0 nm. The presence of PDF peaks at large distances r indicates size distribution of the ruthenium oxide grains. For example, the small peak close to 1.05 nm in Figure 6 for $x = 0.84$ remains at exactly the same position as in the RuO$_2$·0.02H$_2$O sample annealed at 400 °C. This shows that in some parts of the sample,

atomic correlations at this distance are preserved; therefore, in addition to the majority of small crystals there are some larger ones.

In conclusion, despite the apparent amorphousness of the material as measured with conventional XRD, this PDF study indicates that RuO$_2$·xH$_2$O always has well-defined local atomic structural order in the form of nanocrystals, despite large concentrations of structural water. The form of the structure of water between the nanocrystals cannot be assessed by our experiment because the X-ray scattering is dominated by the ruthenium scattering making the low-Z water practically invisible.

Conduction Mechanism. RuO$_2$ is a well-known example of a metallic oxide.[18] Its band structure has been calculated by Mattheiss and others.[19,20] The partly filled conduction band is formed mainly from the Ru 4d orbitals, and is separated from the filled oxygen 2s–2p band. The bottom of the conduction band has a large density of states with the t_{2g} character, although a more detailed description requires three independent subbands due to low symmetry of the Ru site in the rutile structure. The t_{2g} subband is weighted heavily by the nearest-neighbor d–d interactions along the c-axis, and its width is relatively insensitive to the metal–oxygen covalency overlap. The width of the e_g subband, which is higher in energy, is strongly affected by the covalency effects. The present observation that the crystalline RuO$_2$ structure persists to at least 0.5 nm in highly hydrated samples explains the metallic conductivity in RuO$_2$·xH$_2$O. The dispersed nanocrystalline rutile structure preserves the t_{2g} subband and thus metallic conductivity. If the local structure of RuO$_2$·xH$_2$O were truly glassy with significant distribution in the Ru–Ru bonds, the metallic conduction would likely not be maintained, given the narrowness of the t_{2g} subband.

The water can be physisorbed onto RuO$_2$ nanocrystals or chemisorbed as OH, OH$_2$, or OH$_3$ groups. It may be possible to insert hydrogen directly into RuO$_2$ structure as well. The separation between two oxygen atoms of ∼0.25 nm in the a–a plane is ideal for hydrogen insertion. In several proton conductors such as KHCO$_3$,[10] N$_2$H$_5$HC$_2$O$_4$,[11] and Ca$_2$KH$_7$(PO$_4$)2H$_2$O,[23] insertion of hydrogen into such O–O pairs has been established by single-crystal diffraction. An extra electron can be transferred to a Ru atom generating a localized electronic defect state (Ru^{3+}) or be moved to the d-band to create a proton. Thus hydrogen insertion and/or chemisorbtion of water can result in a localized electronic defect state (Ru^{3+}). It should be noted that these defects would be limited to the boundaries between the RuO$_2$ nanocrystals and the structural water.

As opposed to the picture of more homogeneous amorphization or dilution by defect formation, this nanocrystalline model of the structure of RuO$_2$·xH$_2$O implies significant inhomogeneity and a compositional gradient, because it involves definite boundaries between rutile-like nanocrystals and structural water. It suggests that a hydrous RuO$_2$ sample is best viewed as a complex nanocomposite. One component is essentially metallic RuO$_2$ with a structure very close to the rutile structure, but with dispersion in the grain size and porosity down to a sub-nanometer level. The other component is boundaries comprised of chemisorbed water molecules (as OH, OH$_2$, or OH$_3$ groups) in addition to structural water present as H$_2$O. Electron conduction is supported by RuO$_2$ nanocrystals, while proton conduction is supported by the boundaries between the nanocrystals. Due to the dispersive nature of the nanocomposite structure, separate percolation paths must be present between the RuO$_2$ nanocrystals and the hydrous to provide paths for long-range electronic and protonic conduction, respectively. The

electronic and protonic paths are competitive in nature, because more anhydrous RuO$_2$ regions form as water is irreversibly lost from structure, resulting in a decrease in the volume of protonic transport paths and an increase in the metallic conduction paths. As discussed previously,[2,23] the pseudocapacitance and catalytic properties of RuO$_2$·xH$_2$O are optimized when the electronic and protonic transport are balanced. From our EXAFS study,[2] we stated that the electronic and protonic mobility changed with gradual changes in the RuO$_2$·xH$_2$O local structure as structural water is removed. The results of this PDF study now compel us to modify our first theory, and we now assert that the transference numbers for electrons and protons (or their partial conductivities) change with x due to changes in the volume of RuO$_2$ nanocrystals and hydrous boundaries and thus the connectivity of their percolation paths (Figure 8). The conductivity of the metallic RuO$_2$ nanocrystals will always be greater than that of the protonic hydrous boundaries. But if the RuO$_2$ nanocrystals are electronically isolated by hydrous boundaries and not connected in a percolation path, they will not contribute to the specific capacitance (or pseudocapacitance). Thus, the specific capacitance of RuO$_2$·xH$_2$O is optimized when the material is heated near 150 °C and $x \sim 0.5$ because there is high access of both electrons and protons throughout the structure.

Comparison with the EXAFS Results. This nanocomposite structural picture for RuO$_2$·xH$_2$O derived from this PDF study differs from what was determined in a prior EXAFS study. EXAFS analysis of the atomic structure of hydrous ruthenium oxides suggests that the rutile structure of RuO$_2$ becomes strongly disordered with an increasing amount of structural water.[2] For the sample with 0.29 mole of water ($x = 0.29$), the results were attributed to either the decrease in the number of Ru–Ru first (at 0.31 nm) and second nearest neighbors (at 0.354 nm), or to the creation of a range of nearest Ru–Ru distances. In the resulting model, octahedral chains of ruthenium oxide are twisted or distorted with respect to those in the rutile structure. Beyond 0.354 nm (second nearest Ru–Ru distance), this phase would be almost completely disordered. If this EXAFS model were accurate, the PDF analysis would show increased peak width in the PDF at 0.31 and 0.354 nm due to a range of Ru–Ru distances, and complete disorder into lack of any peaks beyond 0.4 nm. However, the PDF analysis shows that peak widths corresponding to the first Ru–Ru distances do not change significantly with variations in the structural water to $x = 0.84$ in the RuO$_2$·xH$_2$O. Moreover, all the peaks up to 0.5 nm are clearly observed, suggesting the presence of RuO$_2$ nanocrystals consisting at least of several unit cells.

The coordination numbers from this PDF study also differs from that of the prior EXAFS analysis. The EXAFS analysis showed that the second shell Ru–Ru coordination (peak at 0.354 nm) is ~2.3 for RuO$_2$·0.29H$_2$O. In this PDF study, the minimum estimate of the second shell Ru–Ru coordination is 4.8 atoms for RuO$_2$·0.35H$_2$O, which is at least 2 times the EXAFS estimate. Although the estimate of this coordination from the X-ray PDF suffers from the overlap of the Ru–Ru peak at 0.354 nm because of the two Ru–O peaks at 0.34 and 0.36 nm, a conservative estimate of the second-shell Ru–Ru coordination number can be calculated assuming the maximum Ru–O contribution of an ideal rutile structure. From the rutile structure (Figure 5), one can calculate that for a single, isolated unit cell, this Ru–Ru coordination number is ~1.78 (16/9). For two unit cells stacked along any axis, it increases to ~2.3 (32/14). For an infinite stack along any axis the limit is 3.2 (16/5). Since our number is at least 4.8 the structure cannot be one-

dimensional and has to extend in more than one axis. Thus our result suggests a three-dimensional structure, albeit with significant dispersion.

The PDF method has several advantages over the EXAFS method. In the EXAFS method the energy dependence of the normalized absorption factor, $\chi(k)$,

$$\chi(k) = \frac{\mu_{\text{obs}}(E)}{\mu_{\text{atom}}(E)} = \sum_i \xi_i(k)e^{ikR_i}, \, E = E_{\text{edge}} + \frac{\hbar^2}{2m}k^2 \quad (4)$$

where $\mu_{\text{obs}}(E)$ and $\mu_{\text{atom}}(E)$ are the absorption coefficients of the sample. For an independent atom at the X-ray energy E, R_i is the distance to the neighbor atom i, and E_{edge} is the energy of the X-ray absorption edge. The Fourier transform of $\chi(k)$ is also called the PDF, however, this should not be confused with the PDF defined by eq 3 and obtained by X-ray or neutron diffraction. The EXAFS interference function, $\chi(k)$, includes the form factor, $\xi_i(k)$, analogous to the X-ray atomic scattering factor, $f(Q)$. This form factor strongly depends on the interatomic distance and becomes rapidly diminished with increasing r. At present, the EXAFS $\chi(k)$ cannot be calculated with sufficient accuracy beyond the first neighbors to deduce the correct structure factor. In comparison, the X-ray scattering factor is well understood and does not depend on the atomic separation, so that it can be easily factored out to recover the structure function $S(Q)$. For this reason the X-ray or neutron PDF can describe the atomic correlation up to large atomic distances, while the EXAFS PDF is reliable only for the first neighbor.

Single-Crystal Study of RuO$_2$−Electrolyte Interface. In recent publications,[25,26] the structure of single-crystal RuO$_2$ surface and adsorbed water layers during CV cycle was studied using X-ray surface diffraction. This basic study contains many interesting results. Among others, the authors describe (100) and (110) surface modification in a sulfuric acid solution. Direct comparison with our results is not appropriate due to in situ nature of that study and very different materials: dispersed rutile-like nanoparticles versus surface of a single crystal. However, there are some interesting points that could be related since a significant volume of a nanocrystal is comprised of a surface. In particular, it was observed[25] for (100) and (110) surfaces that expansion in the top atomic layers occurs in the $\langle 110 \rangle$ directions. The authors suggest that this distortion opens space in the RuO$_2$ structure that could fit molecular water or hydronium ions. Indeed, we observe such distortions in the PDF peak at ~0.63 nm, which corresponds to the base diagonal ($a\sqrt{2}$). This distortion could provide the route for the water/hydronium insertion into the structure and the creation of the Ru–O boundaries.

Conclusions

Hydrous ruthenium dioxide, RuO$_2$·xH$_2$O, is a mixed electron−proton conductor with potential for use in ultracapacitors, direct-methanol fuel cells, and other devices. Determining its atomic structure is important in understanding and controlling its conduction mechanism. The atomic pair-density function (PDF) determined by X-ray scattering of RuO$_2$·xH$_2$O shows that this material is structurally complex. It is not a homogeneous, amorphous medium as suggested by other literature, but rather it is a nanocomposite consisting of dispersed rutile-like nanocrystals with water at the boundaries. The rutile part of the RuO$_2$·xH$_2$O supports electronic conduction, while the structural water at the boundaries transports protons. This dispersive nanostructure implies that charge transport requires establishment of the

interpenetrating percolation paths for electronic and proton conduction. The volume of the electronic and protonic percolation pathways varies as a function of the structural water content of the RuO$_2$·xH$_2$O, and is maximized when the pathways are optimized, as we discussed previously.[23] Such a structural picture explains cyclic voltammetry curves and allows for the presence of the electronic defects at the interface, and suggests that further improvement of performance should be possible by material design to maintain the optimized, nanoscale conduction pathways.

References and Notes

(1) Swider, K. E.; Merzbacher, C. I.; Hagans, P. L.; Rolison, D. R. *Chem. Mater.* **1997**, *9*, 1248.

(2) McKeown, D. A.; Hagans, P. L.; Carette, L. P. L.; Russell, A. E.; Swider, K. E.; Rolison, D. R. *J. Phys. Chem. B* **1999**, *103*, 4825.

(3) Zheng, J. P.; Cygan, P. J.; Jow, T. R. *J. Electrochem. Soc.* **1995**, *142*, 2699.

(4) Jow. T. R.; Zheng, J. P. *J. Electrochem. Soc.* **1998**, *145*, 49.

(5) Trasatti, S.; Lodi, G. In *Electrodes of Conductive Metallic Oxides*, Part B; Trasatti, S., Ed.; Elsevier: Amsterdam, 1981; Chapter 10.

(6) Trasatti, S. *Electrochim. Acta* **1991**, *36*, 225.

(7) Long, J. W.; Stroud, R. M.; Swider-Lyons, K. E.; Rolison, D. R. *J. Phys. Chem. B* **2000**, *104*, 9772.

(8) Rolison, D. R.; Hagans, P. L.; Swider, K. E.; Long, J. W. *Langmuir* **1999**, *15*, 774.

(9) Mills, A.; Giddings, S.; Patel, I.; Lawrence, C. *J. Chem. Soc., Faraday Trans. 1* **1987**, *83*, 2331.

(10) Yamada, A.; Goodenough, J. B. *J. Electrochem. Soc.* **1998**, *145*, 737.

(11) Fletcher, J. M.; Gardner, W. E.; Greenfield, B. F.; Holdoway, M. J.; Rand, M. H. *Chem. Soc. A* **1968**, 653.

(12) Aur, S.; Kofalt, D.; Waseda, Y.; Egami, T.; Wang, R.; Chen, H. S.; Teo, B.-K. *Solid State Commun.* **1983**, *48*, 111.

(13) Egami, T. *Mater. Trans.* **1990**, *31*, 163.

(14) Toby, B. H.; Egami, T. *Acta Crystallogr.* **1992**, *A48*, 336.

(15) Rogers, D. B.; Shannon R. D.; Sleight, A. W.; Gillson, J. L. *Inorg. Chem.* **1969**, *8*, 841.

(16) Shannon, R. D. *Acta Crystallogr.* **1976**, *A32*, 751.

(17) Goodenough, J. B. *Progress in Solid State Chemistry*; Reiss, H., Ed.; Pergamon: Oxford, 1971; Vol. 5.

(18) Mattheiss, L. F. *Phys. Rev. B* **1976**, *13*, 2433.

(19) Glassford, K. M.; Chelikowsky, J. R. *Phys. Rev. B* **1993**, *47*, 1732.

(20) Thomas, J. O.; Tellgren, R.; Olovsson, I. *Acta Crystallogr.* **1974**, *B30*, 1155.

(21) Thomas, J. O.; Liminga, R. *Acta Crystallogr.* **1978**, *B39*, 3686.

(22) Prince, E.; Takagi, S.; Mathew, M.; Brown, W. E. *Acta Crystallogr.* **1984**, *C40*, 1492.

(23) Swider-Lyons, K. E.; Bussmann, K. M.; Griscom, D. L.; Love, C. T.; Rolison, D. R.; Dmowski, W.; Egami, T. In *Solid State Ionic Devices II Ceramic Sensors*; Wachsman, E. D., Weppner, W., Traversa, E., Vanysek, P., Yamazoe, N., Liu, M. L., Eds.; The Electrochemical Society, Pennington, NJ, 2000; Vol. 2000-32, p 148.

(24) Zallen, R. The Physics of Amorphous Solids; John Wiley & Sons: New York, 1983.

(25) Chu, Y. S.; Lister, T. E.; Cullen, W. G.; You, H.; Nagy, Z. *Phys. Rev. Lett.* **2001**, *86*, 3364.

(26) Lister, T. E.; Chu, Y.; Cullen, W.; You, H.; Yonco, R. M.; Mitchell, J. F.; Nagy, Z. *J. Electroanal. Chem.* **2002**, *524−525*, 201.